Whole-body fluorescence lifetime imaging of a tumor-targeted near-infrared molecular probe in mice

Sharon Bloch
Washington University School of Medicine
Department of Radiology
St. Louis, Missouri 63110

Frédéric Lesage
Laura McIntosh
ART Advanced Research Technologies Inc.
2300 Alfred-Nobel Boulevard
St-Laurent, Québec, Canada H4S 2A4

Amir Gandjbakhche
National Institutes of Health
National Institute of Child Health and Human Development
Laboratory of Integrative and Medical Biophysics
Bethesda, Maryland 20892

Kexian Liang
Samuel Achilefu
Washington University School of Medicine
Department of Radiology
St. Louis, Missouri 63110

Abstract. Fluorescence lifetime imaging can provide valuable diagnostic information relating to the functional status of diseases. In this study, a near-infrared (NIR) dye-labeled hexapeptide (abbreviated Cyp-GRD) was synthesized. *In vitro*, Cyp-GRD internalized in nonsmall cell lung cancer cells (A549) without observable cytotoxic or proliferative effects to the cells at a concentration up to 1×10^{-4} M. Time-domain fluorescence intensity and lifetime imaging of Cyp-GRD injected into A549 tumor-bearing mice revealed that the probe preferentially accumulated in the tumor and the major excretion organs. The fluorescence lifetime of the conjugate at the tumor site was mapped, showing the spatial distribution of the lifetime related to its environment. Additionally, fluorescence intensity image reconstruction obtained by integrating the time-resolved intensities enabled the contrast ratios of tumor-to-kidney or liver in slices at different depths to be displayed. The mean lifetime was 1.03 ns for the tumor and 0.80 ns for the liver when averaging those pixels exhibiting adequate signal-to-noise ratio, showing the tumor had a higher lifetime average and reflecting the altered physiopathology of the tumor. This study clearly demonstrated the feasibility of whole-body NIR fluorescence lifetime imaging for tumor localization and its spatial functional status in living small animals. [DOI: 10.1117/1.2070148]

Keywords: fluorescence lifetime imaging; near-infrared molecular probes; time-domain diffuse optical tomography; tumors; mice.

Paper 05094 SSRR received Apr. 12, 2005; revised manuscript received Aug. 18, 2005; accepted for publication Aug. 19, 2005; published online Oct. 4, 2005.

1 Introduction

Advances in molecular biology methods that utilize fluorescence techniques have facilitated the elucidation of the molecular basis of diseases. Fluorescence techniques are attractive because they are highly sensitive, with the capability to detect picomoles of light-emitting fluorophores in heterogeneous mediums.[1–3] As a result, aberrant molecular events that indicate early manifestation of diseases can be assessed by tissue-specific fluorescent-labeled biomolecules. A variety of such molecules that target specific disease mechanisms and markers have been developed and used for *in vitro* and *in vivo* studies of molecular and cellular processes.[4–10]

These studies can be performed by different fluorescence imaging techniques. Among these, fluorescence intensity imaging has been used to localize diseased tissues with high resolution.[2,3,11] Recent studies have shown that fluorescence molecular tomography (FMT) can quantify and localize fluorophore distribution in small animals. In addition, the FMT method has been used to provide valuable information on the functional status of the target tissue.[12]

Another fluorescence imaging technique relies on environment-dependent changes in the fluorescence lifetimes of fluorophores. *In vivo*, tissue heterogeneity within and between organs can lead to changes in fluorophore lifetimes. This heterogeneity is particularly useful for identifying cancerous tissues and differentiating them from normal cells because of the inherent differences in the physiological needs of tumor and normal cells. For example, the differences can be manifested in extracellular pH distribution, blood flow, tissue oxygen and nutrient supply, bioenergetic status, and temperature.[13–15] A combination of these factors can provide measurable changes at the molecular level, which may alter fluorophore lifetimes. Monitoring such changes can be useful in diagnosing malignancies and developing techniques for drug targeting to tumors.

Fluorescence lifetime imaging (FLI) is a valuable tool for localizing diseased tissues and investigating their functional status because the method is less dependent on transient changes in the local concentration of the fluorophore but can be highly sensitive to physiologic environment.[16] Furthermore, artifacts arising from instrumentation can be readily detected and removed from the image when their lifetimes are drastically different from those of the molecular reporter. Unlike intensity measurements, however, FLI measures the energy transfer rate from the excited state of the molecular probe to its immediate environment. Thus, in combination

Address all correspondence to Samuel Achilefu, Department of Radiology, Washington University School of Medicine, 4525 Scott Avenue, St. Louis, MO 63110. Tel: 314-362-8599; Fax: 314-747-5191; E-mail: achilefus@mir.wustl.edu

1083-3668/2005/10(5)/054003/8/$22.00 © 2005 SPIE

with fluorescence intensity measurements, FLI could be useful for simultaneously localizing and quantifying molecular and metabolic processes in living organisms and assessing the functional status of the target tissue.

The primary goal of this study is to demonstrate the feasibility of imaging the distribution of a NIR tumor-specific molecular probe in tumor-bearing mice by fluorescence lifetime method. To be successful, there is a need to develop light-emitting molecular probes that interact with target biomolecules or report on the functional status of diseased tissues with high specificity and selectivity. The molecular probes may possess a lifetime (τ) different from endogenous fluorophores or alter their τ in response to changes in their biological microenvironment. For *in vivo* studies, molecular optical imaging in the near-infrared (NIR) wavelengths is attractive because the contributions of nonspecific endogenous chromophores to the lifetime data are reduced in this region. Consequently, a tumor-specific NIR molecular probe was synthesized to increase the specificity and sensitivity of imaging tumors in living mice. The fluorescence intensity and lifetime maps were obtained by using a time-domain diffuse optical tomography (DOT) imager. The results show that the lifetime map of the probe distribution is comparable to that of the intensity image. Slight differences in the lifetimes of the tumor and liver were observed, indicating the feasibility of localizing cancers and monitoring their functional status by this imaging method.

2 Materials and Methods

All reagents and solvents were obtained from commercial vendors and were used without further purification. Amino acids were purchased from Novabiochem (San Diego, CA). The new peptides were purified and analyzed on a high-performance liquid chromatography (HPLC) system equipped with a tunable UV-visible detector. Analytical (flow rate =0.5 mL/min) and semipreparative (flow rate=10 mL/min) HPLC were performed on C-18 columns and detected at 214 and 254 nm. The compound was purified by using a 30-min linear gradient elution protocol starting from a mixture of 95% A [0.1% aqueous trifluoroacetic acid (TFA)] and 5% B (acetonitrile containing 0.1% TFA) to 30% A and 70% B. The HPLC purity of the molecular probe used for the *in vivo* and *in vitro* studies was >95%. Electrospray ionization mass spectrometry (ESI-MS) analysis was performed on a mass spectrometer (Shimadzu Scientific Instruments, Inc., Columbia, MD).

2.1 *Synthesis of Cypate*

The NIR fluorescent dye Cypate [Fig. 1(a)] was prepared by using an improved method described in the literature.[17] The compound was purified by flash chromatography and about 6 g (85%) of Cypate was obtained, which was further purified by recrystallization from 30% acetonitrile in water to give the desired compound in >95% HPLC purity.

2.2 *Linear Peptide Synthesis and Conjugation with Cypate*

ACT APEX 396 peptide synthesizer was used to prepare the peptide by a standard fluorenylmethyl (Fmoc) protocol,[18] as described previously.[19,20] Conjugation of the dye with the peptide at the *N*-terminus was performed on solid support. After peptide assembly (25 μmol), the *N*-terminal Fmoc group was removed with 20% piperidine in dimethylformamide (DMF). Cypate (75 μmol) was preactivated with diisopropyl carbodiimide (DIC) (125 μmol) in DMF (2 mL) for 20 min and added to the resin-bound peptide. Cleavage of the conjugate from the resin and concomitant removal of the amino acid side-chain protecting groups were accomplished by adding a cleavage mixture (1 mL) of TFA (85%), distilled water (5%), phenol (5%), and thioanisole (5%) to the resin and gently mixing the content for 3 h. The resulting green powder was purified by HPLC to give the desired compound Cypate-Gly-Arg-Asp-Ser-Pro-Lys-OH (Fig. 1(b), abbreviated Cyp-RGD; 6.4 mg, 4.84 μmol) in 19% isolated yield. The molecular probe was characterized by ESI-MS, HPLC, and spectral analysis (Fig. 2).

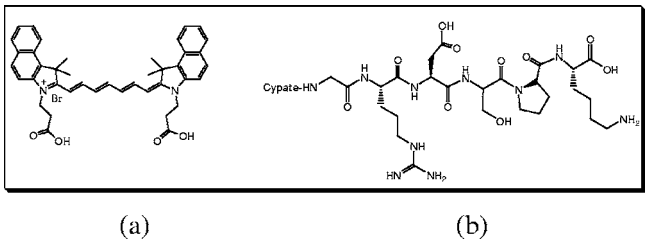

Fig. 1 Structures of (a) Cypate and (b) Cyp-GRD.

2.3 *Cell Culture*

The human nonsmall cell carcinoma cells A549, which are positive for integrin expression,[21] were purchased from ATCC and grown in 75-cm tissue culture flasks or on Lab-Tek chambered slides in Ham's F12K medium with 2 mM L-glutamine supplemented with 1.5 g/L sodium bicarbonate, 10% fetal calf serum, 100 units/ml Penicillin, and 100 units/mL Streptomycin.

2.4 *Cytotoxicity MTT Assay*

Cytotoxicity assays were performed using the 3-(4,5-dimethylthiazol-2-yl)-2,5-diphenyltetrazolium bromide (MTT) *in vitro* toxicology assay kit (Sigma, St. Louis, MO).

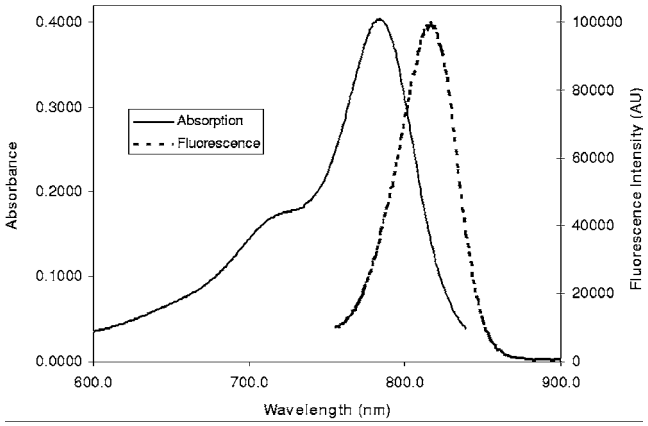

Fig. 2 Absorption and fluorescence emission spectra of Cyp-GRD in 20% aqueous DMSO solution.

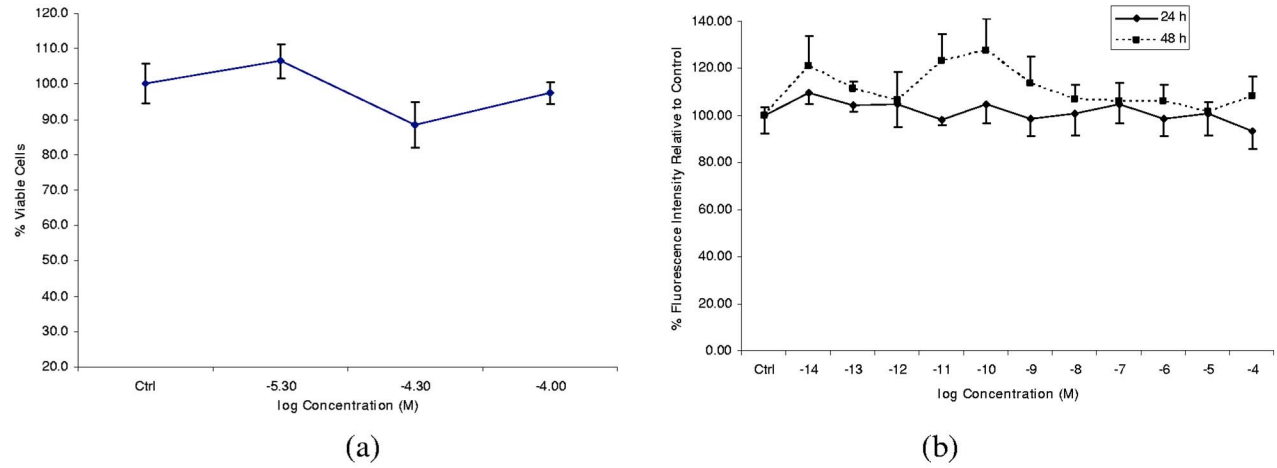

Fig. 3 (a) Measurement of cytotoxicity of Cyp-GRD by the MTT assay at 24 h postincubation. (b) CyQUANT cell proliferation assay.

Briefly, A549 cells were grown on 96 well plates to 75% confluence in phenol red free Dulbecco's Modified Eagle's Medium supplemented with 10% fetal calf serum, 100 units/mL Penicillin, and 100 units/mL Streptomycin. A concentration range of 0 to 125 μM Cyp-GRD was added to each well for a final volume of 100 μL/well and the cells were incubated for 24 h at 37°C in 5% CO_2. After incubation, the media was removed and replaced with 100 μL/well phenol red free medium. Absorbances at 570 nm and 690 nm were measured. MTT (10 μL) was added to each well and the cells were incubated for 2 h. MTT solubilization solution (100 μL, formazan crystals dissolved in 0.04 M HCl in 2-propanol) was added to each well and formazan crystals were dissolved by vigorous mixing. Absorbances at 570 nm and 690 nm were measured. The $\Delta 570$ and $\Delta 690$ were determined by taking the difference of the absorbance before and after the addition of MTT. The percent of viable cells B [Fig. 3(a)] was determined according to:

$$B = \frac{(\lambda_{\Delta 570} - \lambda_{\Delta 690})_{treated}}{(\lambda_{\Delta 570} - \lambda_{\Delta 690})_{untreated}} \times 100 \qquad (1)$$

where $\lambda_{\Delta 570}$ is the absorbance of formazan crystals at 570 nm and $\lambda_{\Delta 690}$ is the background at 690 nm.

2.5 *Cell Proliferation Assay*

Cells were seeded at a concentration of 2.5×10^4 cells/well and grown in 96 well plates in the presence of varying concentrations of Cyp-GRD (0 to 5×10^{-4} M) and incubated for 24 or 48 h. Cell proliferation was measured by using the CyQUANT proliferation assay kit (Molecular Probes, Eugene, OR), as described elsewhere.[22] Briefly, after incubation, the microplate was inverted to remove the media and frozen at −70°C overnight. The microplate was thawed at room temperature and 200 μL of the CyQUANT GR dye in cell-lysis buffer was added to each well. After incubating the mixture for 5 min at room temperature in the dark, the fluorescence was measured using a Synergy HT plate reader (BioTek, Winooski, VT) at 485-nm and 520-nm excitation and emission wavelengths, respectively. The results were expressed as percentages of untreated control [Fig. 3(b)].

2.6 *Animal Preparation*

All *in vivo* studies were performed in compliance with the Washington University Animal Study Committee's requirements for the care and use of laboratory animals in research. Nude mice (18 to 22 g) were anesthetized with a xylazine/ketamine cocktail via intraperitoneal injection and placed in a supine position. The mice were injected subcutaneously in the lower back of the mice with 1×10^6 A549 cells. Tumor masses were palpable at 5 to 7 days postimplant, reaching 5 mm in 10 to 15 days. Prior to injection of the molecular probe, the nude mice were anesthetized as described above. The mice were injected retro-orbitally with the Cyp-GRD in 20% aqueous DMSO solution (100 μL) at a dosage of 0.3 μmol/kg body weight of the rodent.

2.7 *In vivo Optical Imaging Studies*

A schematic diagram of the eXplore Optix imaging system used for this study is shown in Fig. 4. The distribution of Cyp-GRD in the A549 tumor-bearing mice were imaged by positioning the mice on the animal plate, which was heated to 36°C in the eXplore Optix system (ART Advanced Research Technologies Inc., Montreal, Canada). Two-dimensional regions of interest were selected with the aid of a top real-time digital camera. The height of the animal was verified by a side digital camera to ensure the animal was in the correct plane of the imaging optics. The animal was automatically moved into the imaging chamber for scanning. Laser power and count time settings were optimized at 6.71e-005 μW and 0.3 s per point. These parameters were kept constant throughout the imaging sessions.

Excitation and emission spots were raster scanned in 1.5-mm steps over the selected region of interest to generate emission wavelength scans. In the topographic mode, each measurement consisted of a single source-detector pair distanced by 3 mm. Thus in this mode, the number of sources and detectors (source-detector pairs configuration) are equal. There were 216 such points taken for the scans performed in this experiment. This pattern was scanned over the mouse by moving the excitation beam controlled by galvomirrors. A 780-nm pulsed laser diode with a repetition frequency of

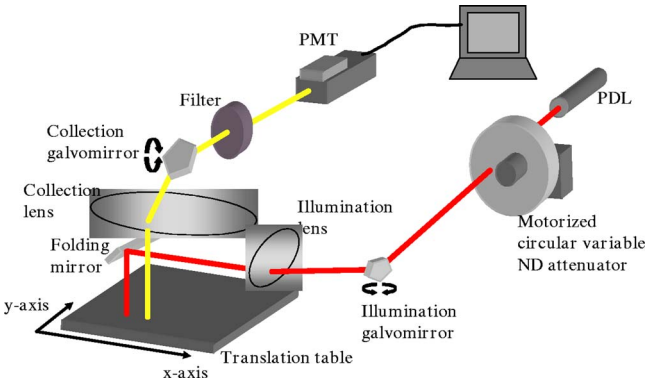

Fig. 4 The animal is positioned on the animal table and a region of interest is selected via a top and side live camera (vision camera). The animal is then translated into the imaging section of the system where the optics are housed. Configured in reflection geometry, the illumination source and detector point(s) are scanned over the region of interest via galvanometer mirrors. Illumination is achieved via a pulsed laser diode. Photons are detected by filtering the appropriate wavelength onto a photomultiplier tube (PMT) detector and through a time-correlated single photon counting board (TCSPC).

80 MHz and a time resolution of 250 ps (PicoQuant GmbH, Berlin, Germany) was used to excite the molecular probe. The fluorescence emission at 830 nm was collected and detected through a fast photomultiplier tube (Hammamatsu, Japan) and a time-correlated single photon counting system (Becker and Hickl GmbH, Berlin, Germany). The data were recorded as temporal point-spread functions (TPSF) and the images were reconstructed as fluorescence intensity and lifetime maps.

The time-resolved fluorescence light intensity detected at the tissue surface is not only dependent on the concentration of fluorophores but is a function of the scattering and absorption coefficients at the excitation and emission wavelengths, as well as the quantum efficiency, fluorescence absorption, and the 3D location of the probes. This is because biological tissues scatter light in the visible and NIR wavelengths. Rather complicated theoretical models have been proposed to describe such processes.[4,23–25] However, for a small source-detector separation, for which the average penetration depth of photons was on the order of a few millimeters and for fluorescence lifetime (on the order of ns), the tail of the TPSF is dominated by the temporal delay caused by the lifetime (Fig. 5). Intuitively, it can be seen that the full-width half maximum (FWHM) of the underlying TPSF, without convolution with the lifetime decay, is much smaller than the lifetime decay when photons travel distances of the order of millimeters and the lifetime is larger than 0.35 ns. This can also be quantified by using a Born approximation to the fluorescence lifetime and simulating TPSF curves.[26] Thus, the resulting measured curves are asymptotically log-linear dominated by the lifetime decay. An estimate of the lifetime of the fluorophore (for each measurement point) is then obtained by measuring the decay of the TPSF and fitting the tail to the form:

$$A \exp(-t/\tau). \tag{2}$$

The effect of the system impulse function has been reported elsewhere,[26] and was shown to have a negligible effect in that range of fluorophore lifetimes. Thus, the map of lifetime images was obtained by simply fitting the log-linear tail of the TPSF and obtaining the characteristic time at each point.

The *in vivo* fluorescence intensity and lifetime of the molecular probe were extracted from the TPSF using different properties of the accumulated curve [Fig. 5(a)]. Since the distances traveled by light were small in this case, the lifetime of Cyp-GRD was fully expressed by the decay of the curve at

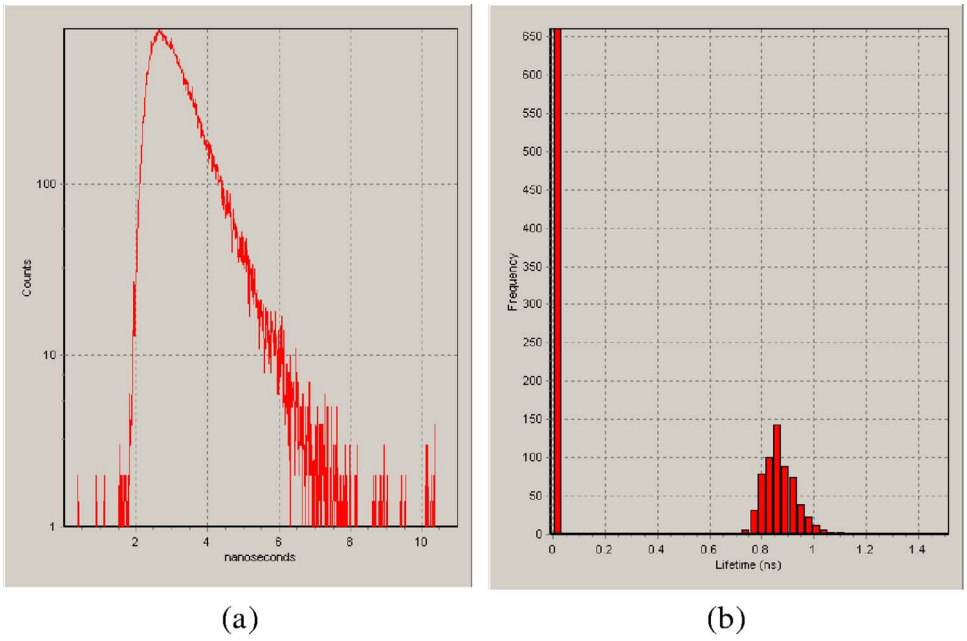

Fig. 5 (a) A typical TPSF curve of Cyp-GRD from a tumor region in a nude mouse at 24 h postinjection. (b) Fluorescence lifetime distribution of Cyp-GRD in a nude mouse at 24 h postinjection. The large signal at 0 ns was obtained from tissues devoid of the probe.

longer times. A histogram representing the distribution of the lifetimes in the image is shown in Fig. 5(b). To obtain this histogram, all of the zero lifetime regions, representing points with no signal from the molecular probe, were discarded. The fluorescence lifetime map was constructed based on the mono-exponential decay [Fig. 5(b)].

TPSFs were also used to reconstruct the 3D concentration of the probe.[27] Reconstruction was performed by discretizing the convolution expression of photon trajectories and lifetime delay and using the temporal moments to create a linear relation between the concentration of the fluorophore and the measurements. The photon trajectories here are modeled by taking into account the first order interaction between the light and the fluorophore (Born approximation). An expression for the Laplace transform of the detected light at position $\vec{r}_d$ given a delta excitation at position $\vec{r}_s$ is

$$\Phi^{\lambda_2}(\vec{r}_s,\vec{r}_d,s) = \int_V d^3\vec{r} G_1(|\vec{r}_s-\vec{r}|,s)\frac{Q_{eff}C(\vec{r})}{1+s\tau}G_2(|\vec{r}_d-\vec{r}|,s). \tag{3}$$

Here, the quantum efficiency is given by $Q_{eff}=q\eta\varepsilon$ where q is the quenching coefficient, η the quantum yield, and ε the extinction coefficient of the fluorophore. Propagation of light at different wavelengths is described by different propagators $[G_1(|\vec{r}_d-\vec{r}|,s)$ and $G_2(|\vec{r}_d-\vec{r}|,s)]$, which are assumed to be equal in this case. By taking derivatives with respect to the Laplace parameter, s, one can build moments of the temporal distribution and show how they can be deconvolved. Full details of the inversion are provided in separate work.[27]

Inversion was performed by minimizing the least square distance between the measurements and the model. The first two moments were used for inversion. To obtain unit consistency, the first moment was renormalized by the intensity in the inversion process. Details of the mathematics and procedures are described by Lam et al.[27] This approach avoided the necessity to compute an instrument calibration factor, with the drawback that a relative concentration was computed.

3 Results and Discussion

3.1 *Tumor-Specific Molecular Probe (Cyp-GRD)*

Indocyanine green (ICG) is the only NIR fluorescent dye currently approved for use in humans by the US Food and Drug Administration. For this reason, it is widely used in contrast agent-mediated NIR optical imaging of human patients.[28,29] Unfortunately, ICG is a nonspecific contrast agent and does not possess reactive functional groups needed to conjugate it with biological carriers to enhance target specificity *in vivo*. These limitations have led to the development of reactive NIR fluorescent dyes, such as Cypate and other carbocyanines for labeling biomolecules. Cypate has similar spectral and biodistribution properties similar to ICG.[20,30] Cypate is primarily excreted by the hepatobiliary system and requires conjugation to a disease-specific carrier to increase the specificity of the molecular probe. Recently, we found that a Cypate-labeled hexapeptide, abbreviated Cyp-RGD (Fig. 1), was preferentially retained in $\alpha_v\beta_3$ integrin receptor-positive tumor (A549).[31] Its retention in this tumor can be inhibited by RGD peptide ligands known to bind with high affinity to this receptor. In contrast to the widely used cyclic RGD peptides, which require an additional cyclization step to obtain the peptide carrier, the hexapeptide used to prepare Cyp-GRD is linear, which facilitates the complete preparation of the tumor-specific molecular probe on solid support. Figure 2 shows that the spectral properties of Cyp-GRD (λ^{ab}_{max} 785 nm, λ^{em}_{max} 817 nm, ε^{ab}_{max}237,680 $cm^{-1}\,Mol^{-1}$) in 20% aqueous dimethyl sulfoxide (DMSO) are similar to those of the non-conjugated dye Cypate (λ^{ab}_{max} 786 nm, λ^{em}_{max} 811 nm, ε^{ab}_{max} 244,400 $cm^{-1}\,Mol^{-1}$), which has been used to prepare several biocompatible optical molecular probes.[19,20] Previous studies have shown that aqueous DMSO solution boosted fluorescence intensity and was well tolerated by rodents.[20,30] The spectral widow of Cyp-GRD allows its use for optical imaging with the fixed wavelength time-domain DOT system. Therefore, Cyp-GRD is attractive for NIR fluorescence lifetime imaging study because of the ease of synthesis, high uptake by the human lung epithelial carcinoma in mice, and suitable spectral properties.

3.2 *Cytotoxicity and Cell Proliferation Effects of Cyp-GRD*

Molecular contrast agents for *in vivo* imaging should enhance the localization and assessment of the functional status of diseases without interfering with the inherent cell growth and functions. Cytotoxicity and proliferation tests provide key information on the suitability of molecular probes for *in vivo* applications. It was necessary to assess these parameters because Cyp-GRD is a new molecular probe. The assays were analyzed at 24 h and 48 h because we typically complete our *in vivo* optical imaging studies within 36 h postinjection of the molecular probe. The MTT test, which determines cell viability, measures the metabolic activity of mitochondrial dehydrogenases.[32] Incubation of varying concentrations of Cyp-GRD with A549 cells for 24 h and subsequent MTT assay showed that the molecular probe was not cytotoxic to these cells up to 1×10^{-4} M [Fig. 3(a)]. Similarly, the CyQUANT cell proliferation assay, which provides cell density information by quantifying the nucleic acids present in a given cell population, showed that Cyp-GRD did not induce cell proliferation at 24 h post-incubation [Fig. 3(b)]. A transient increase in cell density was observed between 1×10^{-11} and 1×10^{-10} M after incubating A549 cells with Cyp-GRD for 48 h. This increase returned to normalcy at 1×10^{-8} M of the probe. Because most imaging studies are expected to be completed within 24 h after administering the probe to living organisms, the MTT and CyQUANT assays demonstrate the biocompatibility of Cyp-GRD for *in vivo* imaging. The results also suggest that a wide range of Cyp-GRD's concentrations are safe for use in animals.

3.3 *Fluorescence Lifetime and Intensity Imaging of Cyp-GRD Distribution in Mice*

Accurate measurement of the distribution of Cyp-GRD in animals by optical methods can be used to localize integrin receptor-positive tumors and characterize tumor heterogeneity. We used a time-domain optical imaging system for this study (Fig. 4). A typical *in vivo* TPSF curve of Cyp-GRD shown in Fig. 5(a) was used to obtain the fluorescence intensity and lifetime maps. A histogram representing the distribu-

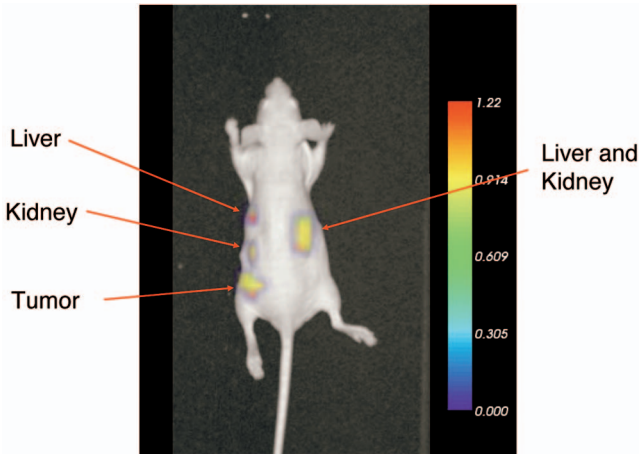

Fig. 6 NIR fluorescence lifetime image of Cyp-GRD distribution in an A549-tumor-bearing mouse at 24 h postinjection.

tion of the lifetimes in the image is shown in Fig. 5(b). Variations of this distribution were observed at different regions of the mice.

The fluorescence lifetime image (FLI) of the whole mouse at 24 h postinjection showed that the molecular probe selectively localized in the target tumor tissue and in the primary excretion organs, the liver and kidneys (Fig. 6). The FLI also delineated the liver from the left kidney but not the right kidney. This image was in agreement with mouse anatomy because the right kidney is closer to the liver than the left kidney. Note that the higher values for lifetime in the left part of the liver were due to noisy signals (lower fluorescence) in that region. Points with inadequate fluorescence to evaluate lifetime were not represented in Fig. 6.

The mean lifetime average of the tumor over eight localized scan points was 1.03 ns, with a minimum τ of 0.76 ns and a maximum τ of 1.5 ns. However, the mean lifetime average of the liver over eight scan points was 0.80 ns, with a minimum τ of 0.74 ns and a maximum τ of 0.85 ns. The tumor had a higher lifetime average, which can be related to

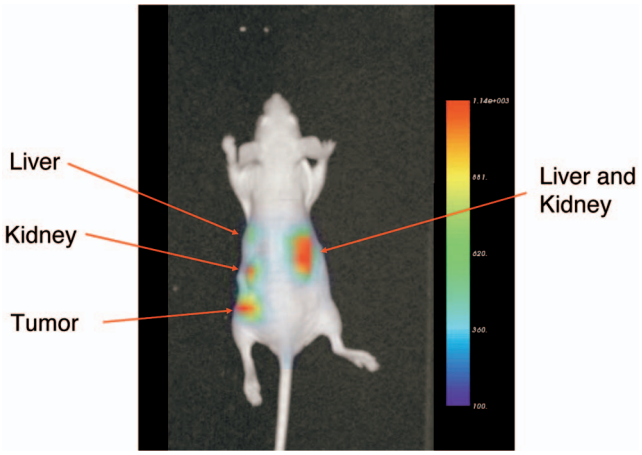

Fig. 7 Fluorescence intensity image of the distribution of Cyp-GRD in an A549 tumor-bearing mouse at 24 h postinjection. Note that the tumor has a significant fluorescence signal.

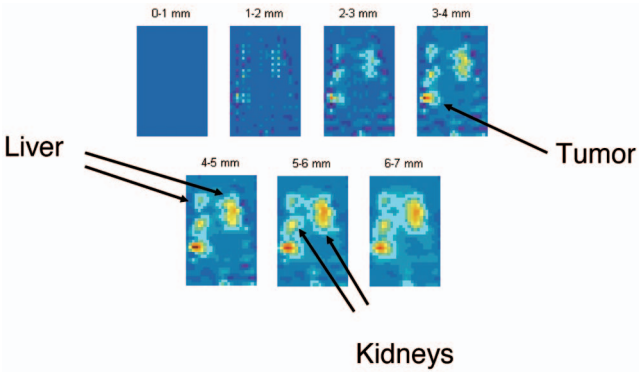

Fig. 8 2D slices of the image from Fig. 6 reconstruction in the Z direction.

higher pH or hypoxic status.[33] A previous study had shown that lifetime of protoporphyrin IX increased from 5 ns in normal tissue to 18 ns in neoplastic tissue.[8] Therefore, lifetime maps can be used to delineate tumor tissues *in vivo*.

A similar FLI biodistribution pattern was obtained by fluorescence intensity imaging (Fig. 7). The molecular probe preferentially localized in the tumor tissue, the kidneys (the major excretion organ), and to some extent the liver. The *ex vivo* image of the organ parts showed that the amount of Cyp-GRD in the liver was low. Optimization of the molecular probe design can lower the amount of the fluorescent probe retained by the kidneys after 24 h of administering the contrast agent.

Figures 8 and 9 were constructed by showing the intensity either in slices cut along the axial axis or through a ray-casting method on the volume. The main advantage of using moments for the inversion was the possibility to deconvolve additively the effects of the impulse response function (IRF) as well as the lifetime decay. To compare tumor and normal tissues, the images were represented as 2D slices in the Z axis, starting at $Z=0$ mm (dorsal skin of the mouse) to about 7 mm deep (Fig. 8).[27,34] The images gave detailed information on the distribution of the molecular probe in the tumor relative to surrounding normal tissues. Particularly, the ratio of the tumor-to-kidney or liver increased in the Z direction, with the largest contrast observed between 3 and 6 mm deep. Table 1

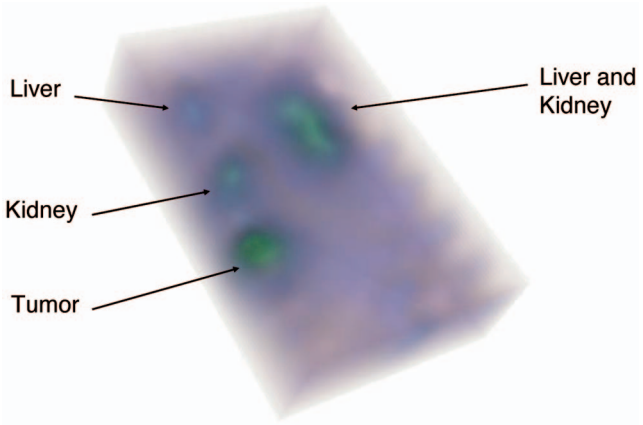

Fig. 9 Volumetric representation through ray-casting of the volume of the tumor and major excretion organs.

Table 1 Parametric information from the reconstruction, the maximal voxel in the region under consideration.

Parameter	Liver	Kidney	Tumor
Depth (mm)	5	4	3
Conc. relative to tumor	0.53	0.88	1

summarizes the depth recovery parametric information obtained by taking the maximal voxel of the volumetric reconstruction for each organ.

A 3D volumetric representation of the probe distribution in the tumor and major excretion organs is shown in Fig. 9. This volumetric rendition of the biodistribution was obtained through ray-casting, which is similar to a maximum intensity projection.

4 Summary

This study has clearly demonstrated the feasibility of using a tumor-specific NIR molecular probe to obtain whole-body FLI in living animals. The FLI image was similar to that of fluorescence intensity, thus providing a complementary method to assess molecular events *in vivo*. Displaying the images in two dimensions allowed the depth profile of the probe distribution to be assessed noninvasively. This representation may be useful for the longitudinal monitoring of tumor response to chemotherapy and radiotherapy. The mean lifetime average of the tumor was 1.03 ns and the liver was 0.80 ns, showing the tumor had a higher lifetime average. Molecular probes that respond to molecular processes are necessary to localize the probe and provide real-time information on the functional status of the target tissue and are being studied. The fluorescence lifetime differences between normal and tumor tissues would be larger when the biodistribution of highly pH- or other environment-sensitive molecular probes are imaged by FLI.

Acknowledgments

This study was supported by the National Science Foundation (BES-01194889) and the National Institutes of Health (R01 CA109754 and R24 CA83060).

References

1. B. Chance, K. Kang, L. He, J. Weng, and E. Sevick, "Highly sensitive object location in tissue models with linear in-phase and antiphase multielement optical arrays in one and 2 dimensions," *Proc. Natl. Acad. Sci. U.S.A.* **90**, 3423–3427 (1993).
2. E. E. Graves, J. Ripoll, R. Weissleder, and V. Ntziachristos, "A submillimeter resolution fluorescence molecular imaging system for small animal imaging," *Med. Phys.* **30**, 901–911 (2003).
3. S. V. Patwardhan, S. R. Bloch, S. Achilefu, and J. P. Culver, "Time-dependent whole-body fluorescence tomography of probe biodistributions in mice," *Opt. Express* **13**, 2564–2577 (2005).
4. A. H. Gandjbakhche, V. Chernomordik, D. Hattery, M. Hassan, I. Gannot, E. Gratton, S. Breusegem, et al., "Tissue characterization by quantitative optical imaging methods," *Technol. Cancer Res. Treat.* **2**, 537–551 (2003).
5. S. Achilefu, "Lighting up tumors with receptor-specific optical molecular probes," *Technol. Cancer Res. Treat.* **3**, 393–409 (2004).
6. E. M. Sevick-Muraca, J. P. Houston, and M. Gurfinkel, "Fluorescence-enhanced, near infrared diagnostic imaging with contrast agents," *Curr. Opin. Chem. Biol.* **6**, 642–650 (2002).
7. J. V. Frangioni, "*In vivo* near-infrared fluorescence imaging," *Curr. Opin. Chem. Biol.* **7**, 626–634 (2003).
8. R. Cubeddu, D. Comelli, C. D'Andrea, P. Taroni, and G. Valentini, "Time-resolved fluorescence imaging in biology and medicine," *J. Phys. D* **35**, R61–R76 (2002).
9. E. Gratton, S. Breusegem, J. Sutin, Q. Ruan, N. Barry, E. M. Sevick-Muraca, G. Lopez, et al., "Fluorescence lifetime imaging for the two-photon microscope: Time-domain and frequency-domain methods," *J. Biomed. Opt.* **8**, 381–390 (2003).
10. P. J. Tadrous, "Methods for imaging the structure and function of living tissues and cells: 2. Fluorescence lifetime imaging," *J. Pathol.* **191**, 229–234 (2000).
11. V. Ntziachristos, J. Ripoll, L. H. V. Wang, and R. Weissleder, "Looking and listening to light: the evolution of whole-body photonic imaging," *Nat. Biotechnol.* **23**, 313–320 (2005).
12. V. Ntziachristos, C. H. Tung, C. Bremer, and R. Weissleder, "Fluorescence molecular tomography resolves protease activity *in vivo*," *Nat. Med.* **8**, 757–760 (2002).
13. R. Cubeddu, G. Canti, A. Pifferi, P. Taroni, and G. Valentini, "Fluorescence lifetime imaging of experimental tumors in hematoporphyrin derivative-sensitized mice," *Photochem. Photobiol.* **66**, 229–236 (1997).
14. M. L. Wahl and D. S. Grant, "Effects of microenvironmental extracellular ph and extracellular matrix proteins on angiostatin's activity and on intracellular ph," *Gen. Pharmacol.—The Vasc. Syst.* **35**, 277–285 (2000).
15. M. J. Boyer and I. F. Tannock, "Regulation of intracellular ph in tumor-cell lines—influence of microenvironmental conditions," *Cancer Res.* **52**, 4441–4447 (1992).
16. J. S. Reynolds, T. L. Troy, R. H. Mayer, A. B. Thompson, D. J. Waters, K. K. Cornell, P. W. Snyder, et al., "Imaging of spontaneous canine mammary tumors using fluorescent contrast agents," *Photochem. Photobiol.* **70**, 87–94 (1999).
17. Y. P. Ye, S. Bloch, and S. Achilefu, "Polyvalent carbocyanine molecular beacons for molecular recognitions," *J. Am. Chem. Soc.* **126**, 7740–7741 (2004).
18. E. Atherton and R. C. Sheppard, "Solid phase peptide synthesis: a practical approach," in *Practical Approach Series*, D. Rickwood and B. D. Hames Eds., Oxford University Press, Oxford, England (1989).
19. S. Achilefu, H. N. Jimenez, R. B. Dorshow, J. E. Bugaj, E. G. Webb, R. R. Wilhelm, R. Rajagopalan, et al., "Synthesis, *in vitro* receptor binding, and *in vivo* evaluation of fluorescein and carbocyanine peptide-based optical contrast agents," *J. Med. Chem.* **45**, 2003–2015 (2002).
20. S. Achilefu, R. B. Dorshow, J. E. Bugaj, and R. Rajagopalan, "Novel receptor-targeted fluorescent contrast agents for *in vivo* tumor imaging," *Invest. Radiol.* **35**, 479–485 (2000).
21. T. M. Odrljin, C. G. Haidaris, N. B. Lerner, and P. J. Simpson-Haidaris, "Integrin alpha v beta 3-mediated endocytosis of immobilized fibrinogen by a549 lung alveolar epithelial cells," *Am. J. Respir. Cell Mol. Biol.* **24**, 12–21 (2001).
22. L. J. Jones, M. Gray, S. T. Yue, R. P. Haugland, and V. L. Singer, "Sensitive determination of cell number using the cyquant (r) cell proliferation assay," *J. Immunol. Methods* **254**, 85–98 (2001).
23. M. J. Eppstein, D. E. Dougherty, D. J. Hawrysz, and E. M. Sevick-Muraca, "Three-dimensional Bayesian optical image reconstruction with domain decomposition," *IEEE Trans. Med. Imaging* **20**, 147–163 (2001).
24. S. R. Arridge, J. C. Hebden, M. Schwinger, F. E. W. Schmidt, M. E. Fry, E. M. C. Hillman, H. Dehghani, et al., "A method for three-dimensional time-resolved optical tomography," *Int. J. Imaging Syst. Technol.* **11**, 2–11 (2000).
25. V. A. Markel and J. C. Schotland, "Symmetries, inversion formulas, and image reconstruction for optical tomography," *Phys. Rev. E* **70**, 056616 (2004).
26. G. Ma, N. Mincu, F. Lesage, P. Gallant, and L. McIntosh, "System irf impact on fluorescence lifetime fitting in turbid medium," *Proc. SPIE* **5699**, 263–273 (2005).
27. S. Lam, F. Lesage, and X. Intes, "Time domain fluorescent diffuse optical tomography," *Proc. SPIE* **5578**, 179–187 (2004).
28. M. M. Haglund, M. S. Berger, and D. W. Hochman, "Enhanced optical imaging of human gliomas and tumor margins," *Neurosurgery* **38**, 308–317 (1996).
29. V. Ntziachristos, A. G. Yodh, M. Schnall, and B. Chance, "Concurrent MRI and diffuse optical tomography of breast after indocyanine

green enhancement," *Proc. Natl. Acad. Sci. U.S.A.* **97**, 2767–2772 (2000).
30. J. E. Bugaj, S. Achilefu, R. B. Dorshow, and R. Rajagopalan, "Novel fluorescent contrast agents for optical imaging of *in vivo* tumors based on a receptor-targeted dye-peptide conjugate platform," *J. Biomed. Opt.* **6**, 122–133 (2001).
31. S. Achilefu, S. Bloch, M. A. Markiewicz, T. X. Zhong, Y. P. Ye, R. B. Dorshow, and B. Chance, et al., "Synergistic effects of light-emitting probes and peptides for targeting and monitoring integrin expression," *Proc. Natl. Acad. Sci. U.S.A.* **102**, 7976–7981 (2005).
32. K. P. Putnam, D. W. Bombick, and D. J. Doolittle, "Evaluation of eight *in vitro* assays for assessing the cytotoxicity of cigarette smoke condensate," *Toxicol. in Vitro* **16**, 599–607 (2002).
33. P. A. Schornack and R. J. Gillies, "Contributions of cell metabolism and h+ diffusion to the acidic ph of tumors," *Neoplasia* **5**, 135–145 (2003).
34. D. Hall, G. B. Ma, F. Lesage, and W. Yong, "Simple time-domain optical method for estimating the depth and concentration of a fluorescent inclusion in a turbid medium," *Opt. Lett.* **29**, 2258–2260 (2004).